Undrained Shear Strength of Clay and Stability of Submarine Slope Undergoing Rapid Deposition

粘土의 非排水 剪斷强度와 持續性堆積에 의한 海底斜面의 安定性

Kim, Seung-Ryull*

金 承 烈

要 旨

本 硏究는 人工軟弱粘土를 試料로 하여 未壓密粘土의 非排水 剪斷强度가 壓密過程에서 어떻게 變異되는가를 考察하고 그 結果를 粘土粒子가 相當한 速度를 가지고 持續的으로 堆積하고 있는 海底斜面에 適用하여 斜面의 安定性을 檢討하였다.

非排水 三軸壓縮 剪斷强度는 壓密度가 增加함에 따라 拋物線을 그리며 增加하였고 有效應力과는 不可分의 關係가 있음이 考察되었다. 斜面安定 檢討에는 實驗結果値들이 有限要素 프로그램에 入力되었으며 흙의 壓縮性과 透水係數도 壓密度에 따라 變化시켰다. 堆積率, 壓密度間의 關係와 斜面崩壞時點과 移動土量豫測圖가 提示되었다.

Abstract

A series of CU triaxial compression tests were conducted to investigate the variation of undrained shear strength of underconsolidated clay at different degrees of consolidation. The soil samples were artificially made by one-dimensional consolidation using soft Bangkok Clay. The test results showed that the undrained shear strength of clay parabolically increased convexing downward with increasing degrees of consolidation. However, all the measured shear strength were unanimously related to the effective stress. These experimental results were used in the numerical analysis.

A finite element computer program was developed to investigate the stability of submarine slope undergoing rapid deposition taking into account the variation in soil compressibility and permeability during the consolidation process. The relationships of degree of consolidation with time as a function of rate of deposition and angle of slope were established. A method of predicting the time of slope failure and the volume of moving mass of soil was also made.

1. Introduction

The underconsolidated clay is defined as 'The clay which is in a progressive state of consolidation'. The underconsolidation in marine sediments is associated with the phenomenon

* 正會員, AIT, 박사과정

of rapid deposition and delay in pore pressure dissipation under this increased total stress.[8] On the continental shelves off large deltas, rapid progradation, deposition, and low permeability are the primary agents responsible for the high degree of underconsolidation. For instance, the Mississippi River discharges 1.5 million metric tons of sediments a day. More than 50% of this amount consists of materials of less than 5 microns in diameter.[5]

The stability of the sediments on a given slope basically depends on the shear strength of the sediments on a given slope basically depends on the shear strength of the sediments and the rate of increase of this strength with burial depth. A slope fails when the shearing stress along the potential surface of sliding exceeds the shearing resistance along this surface. The underconsolidated clay mass has time-dependent characteristics of shear strength. Theoretical models of this mechanism have been postulated by several researchers.[3,7,10] The key characteristic of underconsolidated soils on the stand-point of stability is the amount and distribution of excess pore pressure.

The occurence of submarine landslides has been frequently reported.[2,5,6,9] Such landslides often cause serious damage to structures located at the upper edge of the slope, breaking of submarine cables and pipes, changes in topography of seafloor, and other offshore facilities. Thus, it is essentially needed to identify the potentially unstable deposits such as large mass of submarine deposit which is continuously growing. At present, there exists a need for fundamental studies on the behaviours of underconsolidated seabed clays.

This study consists of two parts, namely

(i) laboratory tests on artificially consolidated clays in order to investigate the behaviours of underconsolidated clay with different degrees of consolidation under triaxial loading.

(ii) numerical analysis of slope stability of submarine deposit which is growing, using the finite element method.

By combination of experimental results and numerical analysis, the characteristics of potentially unstable submarine deposit can be identified.

2. Sample Preparation and Testing Procedure

2.1 Preparation of the Artificial Clay Samples

An artificially consolidated clay samples were used in order to eliminate the effects of stress history and anisotrophy of the soil, and obtain homogeneous, uniform soft clay samples. The clay which has been called 'Soft Bangkok Clay' (liquid limit 95%, plastic limit 30%, and specific gravity 2.69) was thoroughly remoulded with fresh water to a slurry of 250% water content. The slurry was one dimensionally consolidated in a special cylinder to a maximum pressure of 49 KN/m^2

Subsequently, the samples were extruded and trimmed (height 7.13 cm, diameter 3.60 cm), and were isotropically reconsolidated under the effective pressure of 108 KN/m^2. This state of sample is considered as a zero degree of consolidation for the subsequent series of consolidation pressure. The typical consolidation-time history is shown in Fig. 1. The sample preparation and testing procedure are described in detail by Kim.[4]

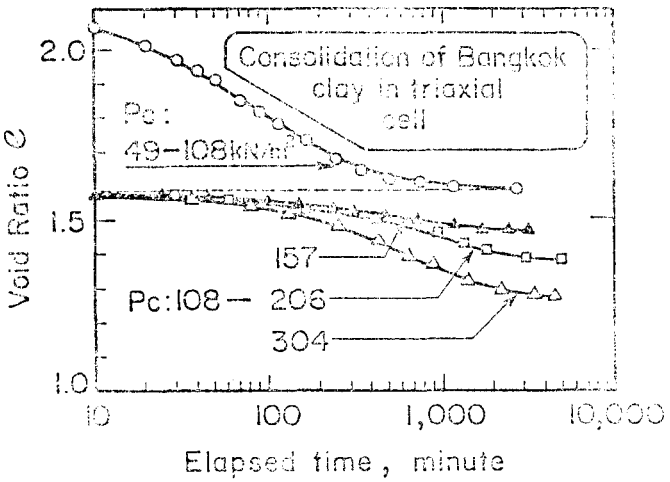

Fig. 1 Compression-Time history in triaxial cell

2.2 Triaxial Compression Test

Special precautions were taken to reduce the effects of non-uniformity in deformation by the use of lubricated ends. During saturation, a slightly higher cell pressure than the back pressure was maintained. Throughout the consolidation process, the horizontal movement and rotation of the top of the specimen were not allowed by using a special cap (Kim[4]). Leakage was virtually eliminated by the use of silicone grease.

The degree of consolidation was defined in this study as follows:

$$\text{Degree of Consolidation } U(\%)=\frac{(\text{Volume change at time } T)\times 100}{(\text{Volume change at end of primary consolidation})}$$

3. Results of Experimental Investigation

3.1 Uniformity of the Artificial Samples

On visual examination, the artificial clay samples were quite uniform without any lamination of silt or air pockets. There were no remarkable variations in initial properties of the soil after artificial consolidation. It was inevitable that the sample produced artificially in the laboratory had a variation in water content among consolidation batches. However, the average differences were as small as about 2% (80±1%).

The average variation in water content between center and side at the top and bottom was about 4%. However, the water content which was measured at the top and bottom of the triaxial specimen after trimming was almost the same. The small variation of water content in radial direction of the specimen caused bending of the specimen during consolidation in the triaxial cell. The special cap eventually prevented the bending failure of clay sample.

3.2 Compression Characteristics

Figure 2 shows the compression indices, C_c, which slightly increases with increase of the degree of consolidation. Fig. 3 verifies that the void ratio is a function of the effective stress.

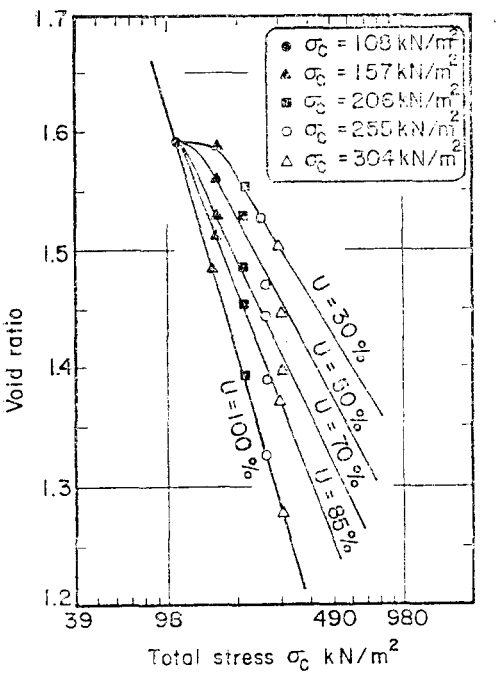

Fig. 2 Compression index versus degree of consolidation

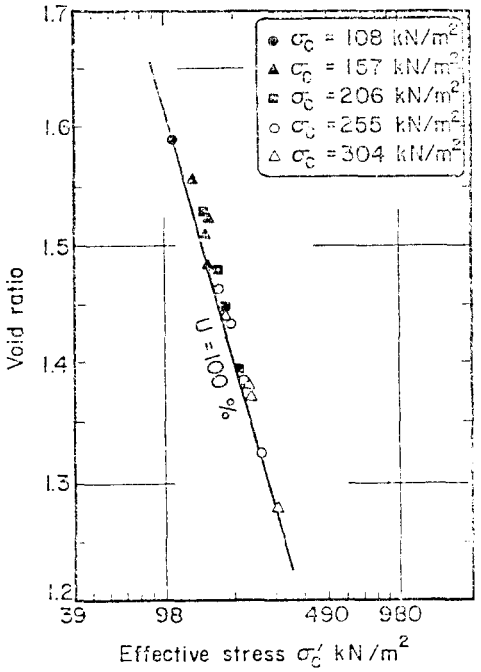

Fig. 3 Void ratio versus effective stress

The change in void ratio, however, does not exactly follow the 100% consolidation line. This might mean that the strength does not linearly increase with the degree of consolidation.

3.3 Deviator Stress-Strain Characteristics

The relationship between shear stress and axial strain of the strain-controlled undrained tests with the degree of consolidation of 100% and 50% are shown in Fig. 4 and Fig. 5 respectively. The comparison of the two figures indicates that the rate of increment of deviator stress due to increased total stress at 50% consolidation is less than that of 100% consolidation.

Theoretically, there exits a unique relationship between the normalized stress and the axial strain for a particular soil. However, when the deviator stresses at different degrees of

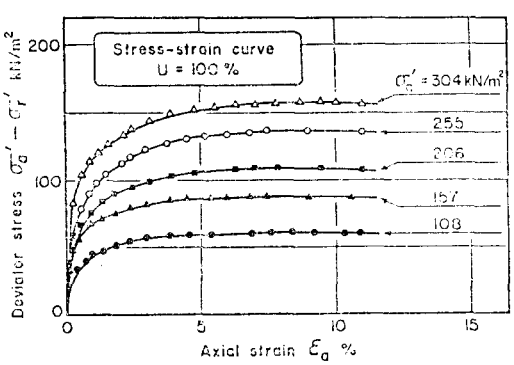

Fig. 4 Deviator stress and axial strain at U=100%

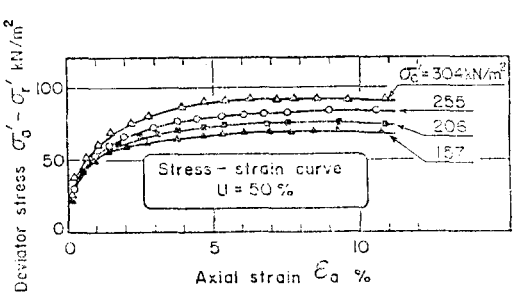

Fig. 5 Deviator stress and axial strain at U=50%

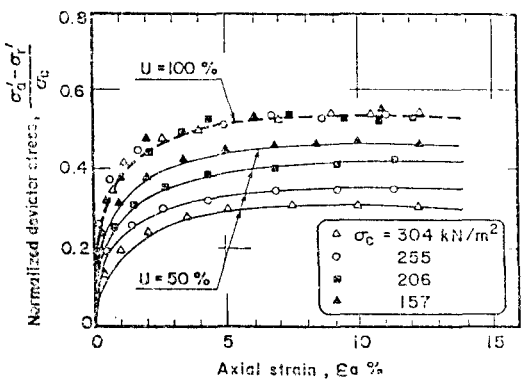

Fig. 6 Normalized deviator stress by total stress with degree of consolidation

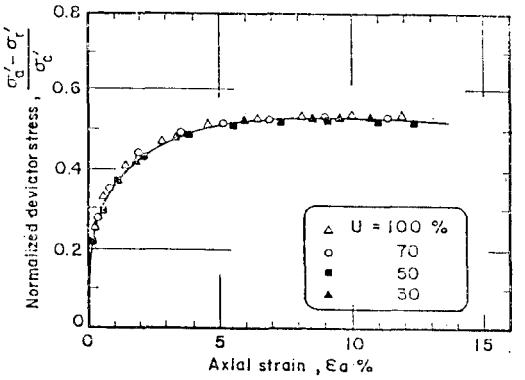

Fig. 7 Normalized deviator stress by effective stress before shearing

consolidation are normalized by their total consolidation stress, the uniquely normalized behaviour is not seen like the case of 100% consolidation in Fig. 6. It means that at lower degrees of consolidation, the deviator stress of soil does not increase in proportion to the total consolidation pressure. On the contrary, when the deviator stresses are normalized by their effective stresses before shearing, the normalized behaviour is apparent (Fig. 7). These show that the behaviours of soil during shear are not affected by their total consolidation stress, but they are significantly influenced by their initial effective stress.

3.4 Strength-Degree of Consolidation

Although Fig. 8 indicates that a higher consolidation pressure yields a higher strength at the same degree of consolidation, a unique normalized relationship with their consolidation pressure was not found. The relationship between normalized strength increments and degree of consolidation is shown in Fig. 9. The normalized strength increment is defined as,

$$\text{Normalized strength increment } SI=\frac{(\text{Strength at } U)-(\text{Strength at } U=0\%)}{(\text{Strength at } U=100\%)-(\text{Strength at } U=0\%)}$$

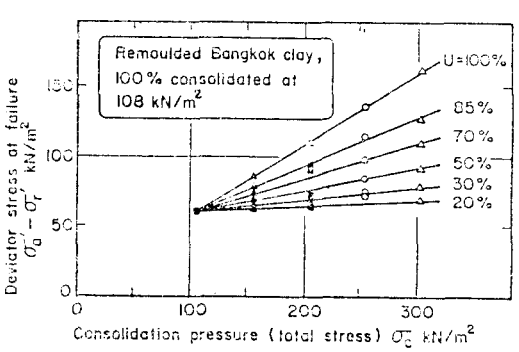

Fig. 8 Deviator stress and consolidation pressure with degree of consolidation

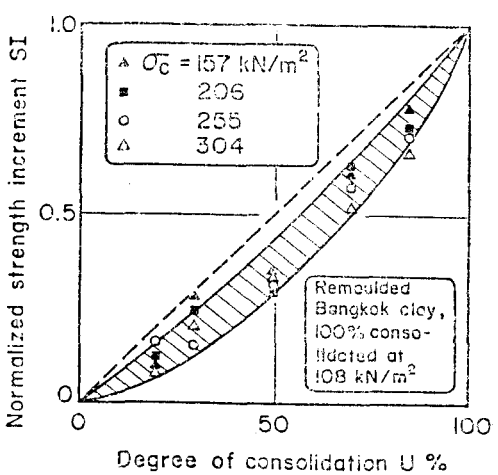

Fig. 9 Normalized strength increment and degree of consolidation

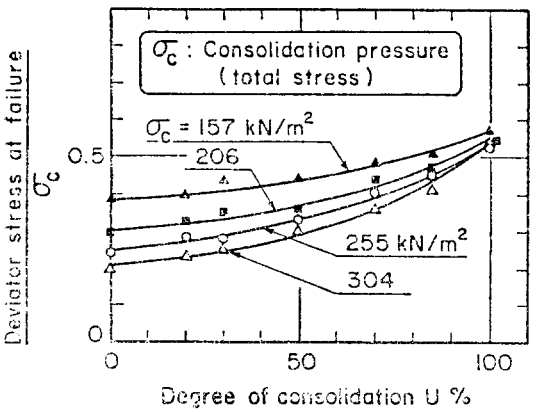

Fig. 10 Normalized daviator stress and degree of consolidation

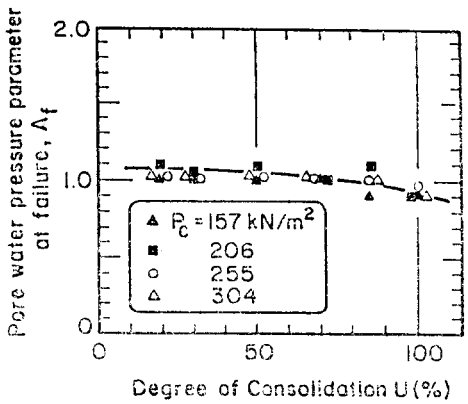

Fig. 11 Pore pressure parameter A_f and degree of consolidation

Fig. 9 clearly shows that the undrained shear strength does not linearly increase with the degree of consolidation. The strength increment tends to slightly decrease with increase of consolidation pressure.

Figure 10 also shows that there is no normalized behaviour between deviator stress and the degree of consolidation when the deviator stresses are normalized by their total consolidation stress. At zero degree of consolidation, for a saturated soil, the soil sample has a equal effective stress leading to equal strength irrespective of total consolidation pressure, σ_c. However, at U=100%, the total stress is equal to the effective stress which yields the corresponding strength. During the consolidation process, the higher consolidation pressure yields more rapid increment of strength than that by lower consolidation pressure. Eventually the normalized strength behaviour is shown at U=100% state.

3.5 Pore Pressure and Parameter A

At a lower degree of consolidation, the development of pore pressure during shearing is not significantly influenced by its amount of total consolidation pressure. It was found that the effects of total stress on the development of pore pressure decrease with decreasing degrees of consolidation due to the fact that their effective stresses are approaching 108KN/m². The higher consolidation pressure generates the higher rate of development of pore pressure (with respect to time) compared with those of lower stress level at the same degree of consolidation. Thus the initial effective stress which the sample had just before shearing greately affect the development of pore pressure during shearing.

The variation of pore pressure parameter A slightly increases with decreasing degrees of consolidation without showing the unique normalized behaviour. Fig. 11 shows that the pore pressure parameter at failure, A_f, slightly increases with decrease of degree of consolidation.

3.6 Stress Path and Strength Envelope

The peak effective stress point having different consolidation pressures for all degrees of consolidation closely fall on the unique line. The ratio of deviator stress to effective mean

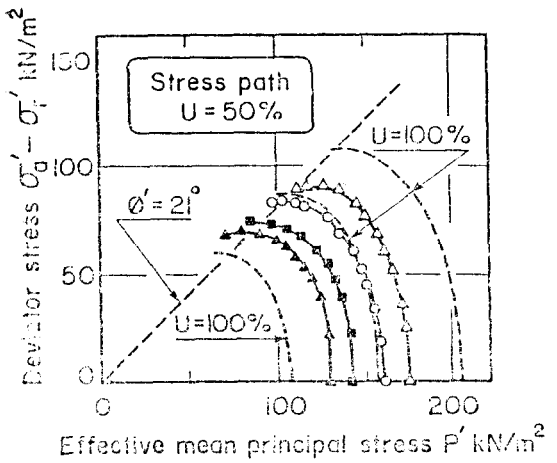

Fig. 12 Deviator stress and effective mean principal stress $P'=1/3(\sigma_1'+2\sigma_3')$ at $U=50\%$

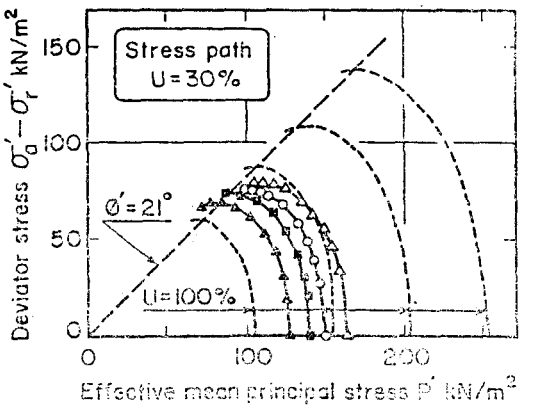

Fig. 13 Deviator stress and effective mean principal stress $P'=1/3(\sigma_1'+2\sigma_3')$ at $U=30\%$

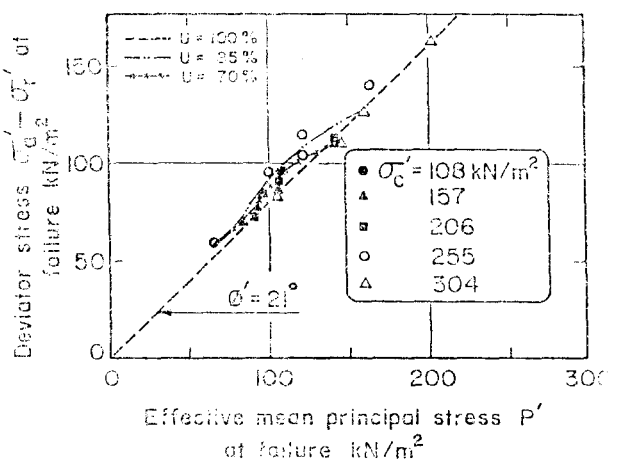

Fig. 14 Deviator stress and effective mean principal stress at failure

principal stress, q/p', was 0.81, and $\phi'=21°$. The shape of stress path is also similar to those of samples isotropically consolidated by the current effective stress (Figs. 12, 13). Particularly, there is a slight tendency in which the lower U causes more pore pressure for the equal initial effective stress.

It is interesting to note in Fig. 14 that the soil has nearly the same effective strength parameter regardless of their degree of consolidation and consolidation pressure. This characteristic is used for the following stability analysis of underconsolidated clays.

4. Numerical Assessment for the Submarine Deposit

4.1 One-dimensional Consolidation Equation

For the one-dimensional condition based on the assumptions that the flow of the water occurs

only in the vertical direction, the pore pressure varies linearly with depth, and there is no horizontal strain, the equations governing consolidation are as follows:

$$\frac{k(1+e)}{\gamma_w a_v}\cdot\frac{\partial^2 u_e}{\partial z^2}=-\frac{\partial \sigma_v'}{\partial t} \tag{4.1}$$

where, k : Darcy's coefficient of permeability

a_v : coefficient of compressibility

u_e : excess pore pressure

z : coordinate in vertical direction

σ_v' : effective stress

Equation(4.1) can be rewritten in terms of total stress and pore pressure instead of effective stress. Eq(4.2) is well known as Terzaghi's consolidation equation.

$$\frac{\partial u_e}{\partial t}=C_v\frac{\partial^2 u_e}{\partial z^2}+\frac{\partial \sigma_v}{\partial t} \tag{4.2}$$

where,
$$C_v=\frac{k(1+e)}{\gamma_w a_v}=\frac{k}{\gamma_w m_v}$$

σ_v : total stress

m_v : coefficient of volume change

4.2 Solution of Consolidation Equation

The Eq. (4.2) is written as,

$$\frac{\partial u}{\partial t}=C_v\frac{\partial^2 u}{\partial z^2}+\frac{dp}{dt} \tag{4.3}$$

where, u : excess pore pressure

(dp/dt) : rate of deposition in terms of total stress

4.2.1 Boundary Condition

The deposit is divided into finite layers. It is assumed that the pore pressure in each layer varies linearly. The following boundary conditions are used.

i) Excess pore water pressure at the top of the deposit is zero.

ii) $(\partial u/\partial z)_{n+1}=0$ (impervious boundary at the bottom).

4.2.2 Equation for the Element

The ground is divided into 'n' layers each having a thickness of h. u_i, η are the pore pressure at node i and local coordinate respectively.

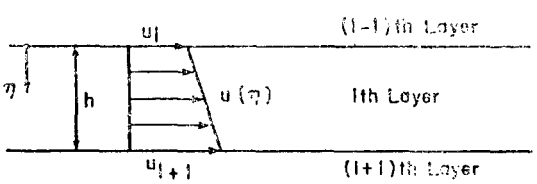

$$u=\left[1-\frac{\eta}{h},\ \frac{\eta}{h}\right]\begin{Bmatrix}u_i\\u_{i+1}\end{Bmatrix} \tag{4.4}$$

$$\frac{\partial u}{\partial z}=\frac{\partial u}{\partial \eta}=\left[-\frac{1}{h},\ \frac{1}{h}\right]\begin{Bmatrix}u_i\\u_{i+1}\end{Bmatrix} \tag{4.5}$$

Now Equation (4.3) is applied to each layer by multiplying an arbitrary function, $W(\eta)$, and integrating for local coordinate, η

$$\left[C_v\frac{\partial u}{\partial \eta}W(\eta)\right]_0^h-\int_0^h\left\{C_v\frac{\partial u}{\partial \eta}\frac{\partial W}{\partial \eta}+\left(\frac{\partial u}{\partial t}-\frac{dp}{dt}\right)W(\eta)\right\}d\eta=0 \tag{4.6}$$

Let's introduce,

$$F_i(i)=-C_v(i)\frac{\partial u}{\partial \eta}\ \text{at}\ \eta=0$$
$$F_{i+1}(i)=C_v(i)\frac{\partial u}{\partial \eta}\ \text{at}\ \eta=h \tag{4.7}$$

Equations (4.4), (4.5) and (4.7) are substituted into Equation (4.6), and it can be rearranged as Eq. (4.8) since it is valid for any W_i and W_{i+1}

$$\begin{bmatrix}F_i(i)\\F_{i+1}(i)\end{bmatrix}=\frac{C_v}{h}\begin{bmatrix}1&-1\\-1&1\end{bmatrix}\begin{Bmatrix}u_i\\u_{i+1}\end{Bmatrix}+\frac{h}{6}\begin{bmatrix}2&1\\1&2\end{bmatrix}\begin{Bmatrix}\dot{u}_i\\\dot{u}_{i+1}\end{Bmatrix}-\frac{h}{2}\frac{dp}{dt}\begin{bmatrix}1\\1\end{bmatrix} \tag{4.8}$$

Introducing m_v in each layer into equation (4.8).

$$\begin{bmatrix}m_vF_i(i)\\m_vF_{i+1}(i)\end{bmatrix}=\frac{m_vC_v}{h}\begin{bmatrix}1&-1\\-1&1\end{bmatrix}\begin{Bmatrix}u_i\\u_{i+1}\end{Bmatrix}+\frac{m_vh}{6}\begin{bmatrix}2&1\\1&2\end{bmatrix}\begin{Bmatrix}\dot{u}_i\\\dot{u}_{i+1}\end{Bmatrix}-\frac{m_vh}{2}\frac{dp}{dt}\begin{bmatrix}1\\1\end{bmatrix} \tag{4.9}$$

Here, $m_vF_i(i)$ and $m_vF_{i+1}(i)$ are the discharge velocity at the top of layer (i) and $(i+1)$ respectively. For continuity of water flow, the summation of the discharged amount of water at node i should equal to zero, Thus,

$$m_{v(i-1)}F_i(i-1)+m_{v(i)}F_i(i)=0 \tag{4.10}$$

From Equations (4.9) and (4.10), Equation (4.11) for $i=2,3\cdots N$ is obtained.

$$\left[-\left(\frac{m_vC_v}{h^2}\right)_{i-1},\ \frac{(m_vC_v)_{i-1}+(m_vC_v)_i}{h^2},\ -\left(\frac{m_vC_v}{h^2}\right)_i\right]\begin{Bmatrix}u_{i-1}\\u_i\\u_{i+1}\end{Bmatrix}$$
$$+\left[\left(\frac{m_v}{6}\right)_{i-1},\ \frac{(m_v)_{i-1}+(m_v)_i}{3},\ \left(\frac{m_v}{6}\right)_i\right]\begin{Bmatrix}\dot{u}_{i-1}\\\dot{u}_i\\\dot{u}_{i+1}\end{Bmatrix}=\frac{(m_v)_{i-1}+(m_v)_i}{2}\frac{dp}{dt} \tag{4.11}$$

At the top of the deposit, $u_1=0$. Imaginary nodal point is used by assuming $u_0=-u_2$. Thus, skew symmetric distribution of pore water pressure, u, is used.

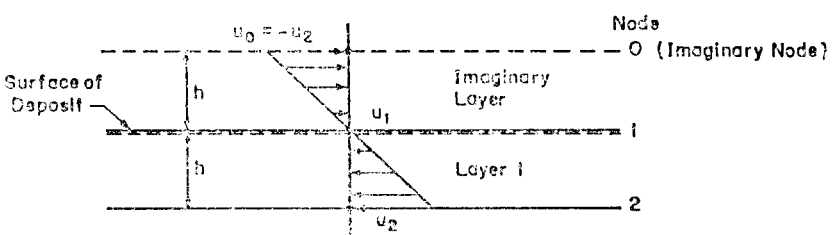

Then the equation at node $i=1$ is obtained by using equation (4.11) and imposing $u_0=-u_2$. It is resonable to say that the imaginary value of $m_{v0}=m_{v1}$, $C_{v0}=C_{v1}$, $(dp/dt)_0=-(dp/dp)_1$. Hence,

$$\frac{C_{v1}}{h^2}u_1+\frac{1}{3}\dot{u}_1=0 \tag{4.12}$$

At the bottom $(\partial u/\partial z)=0$. To provide this condition, imaginary layer $n+1$ and nodal point $n+2$ are assumed. The symmetric distribution of pore pressure is used by assuming $u_n=u_{n+2}$. It gives a $(\partial u/\partial z)=0$ condition at the bottom of deposit.

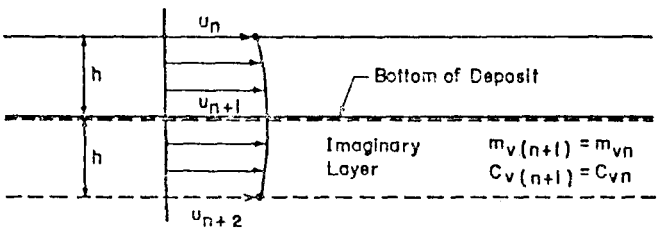

Equation (4.11) for $i=n+1$ with $u_n=u_{n+2}$ is as follows:

$$\left[-\frac{C_{vn}}{h^2},\ \frac{C_{vn}}{h^2}\right]\begin{Bmatrix}u_n\\u_{n+1}\end{Bmatrix}+\left[\frac{1}{6},\ \frac{1}{3}\right]\begin{Bmatrix}\dot{u}_n\\\dot{u}_{n+1}\end{Bmatrix}=\frac{1}{2}\frac{dp}{dt} \tag{4.13}$$

Equations (4.11), (4.12) and (4.13) are employed to calculate the pore pressure at every node $(u_1, u_2 \cdots u_{n+1})$. These equations are assembled in the following matrix form for the deposit having n layers.

$$[K]\{u\}+[C]\{\dot{u}\}=[B]\ (dp/dt) \tag{4.14}$$

4.2.2 Direct Integration with Respect to Time

The direct integration with respect to time is based on the following assumption that the pore pressure, $\{u\}$, at time t and at time $(t+\Delta t)$ have the following relation.

$$\{u\}_{(t+\Delta t)}=\{u\}_{(t)}+\{(1-\beta)\{\dot{u}\}_{(t)}+\beta\{\dot{u}\}_{(t+\Delta t)}\}\Delta t \tag{4.15}$$

Equation (4.14) can be written for time t and time $(t+\Delta t)$ respectively.

$$[K]\{u\}_{(t)}+[C]\{\dot{u}\}_{(t)}=[B]\ (dp/dt) \tag{4.16}$$

$$[K]\{u\}_{(t+\Delta t)}+[C]\{\dot{u}\}_{(t+\Delta t)}=[B]\ (dp/dt) \tag{4.17}$$

Then Eq. (4.16) and Eq. (4.17)are multiplied by $(1-\beta)$ and β respectively and added together. Eq. (4.15) is used to eliminate time derivatives of pore pressure. The result is

$$[P]\{u\}_{(t+\Delta t)}=[R]\{u\}_{(t)}+[B]\frac{dp}{dt} \tag{4.18}$$

where, $[P]$: $(1/\Delta t)[C]+\beta[K]$

$[R]$: $(1/\Delta t)[C]+(1-\beta)[K]$

$\{u\}_{(t+\Delta t)}$: pore pressure at each node at time $(t+\Delta t)$

$\{u\}_{(t)}$: pore pressure at each node at time t

(dp/dt) : rate of deposition

4.3 Simulation of Time-Dependent Thickness into Finite Element

The actual situation in which the thickness of deposit increases at constant rate, can be simulated in the FEM analysis by using step-by-step approach as shown in Fig. 15.

At Step 0 in Fig. 15 the existing deposit is divided into N layers and the initial stress conditions in each layer are calculated based on the given properties and behaviours of sediments. The hydrostatic pressure is not taken into account. For the following Step 1, the increment of thickness, $Hs=\alpha H_0$, is determined by the given parameter α, and converted into corresponding load ΔP, for later use.

The total load corresponding increment of thickness Hs, is divided into resonably small increments. Now this small increment of load is applied to the finite element model step-by-step for the time t_1 of which the required time to produce the thickness Hs. The induced stress and pore pressure due to each increment of load are calculated throughout the layer, and they are

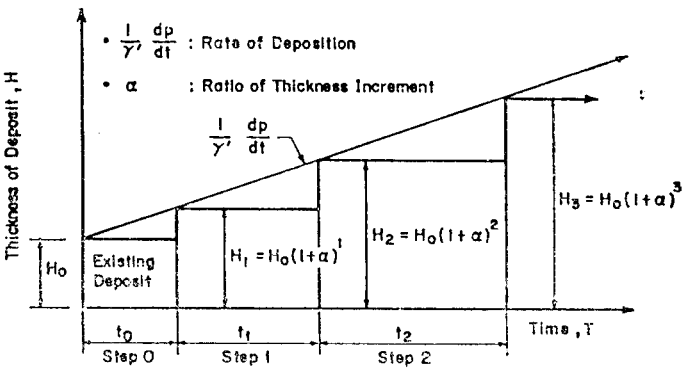

Fig. 15 Schematic diagram on the transformation of new sedimentation load to finite element

added to the initial values.

As the load application is complete the increment of thickness, Hs, is added to the initial thickness H_0. This updated thickness $\{H_1=H_0\ (1+\alpha)\}$ with newly obtained stresses are considered as the initial stage of the next Step 2. This series of steps are repeated until the failure of slope is encountered or the given period of assessment terminated.

If the value of α and the load-increment are small enough, then the simulation in the program is more realistic.

5. Results of Numerical Analysis

5.1 Parameters

The relationship between void ratio and effective stress and the strength parameters which were obtained through the experiments of this study were used. It was considered that the

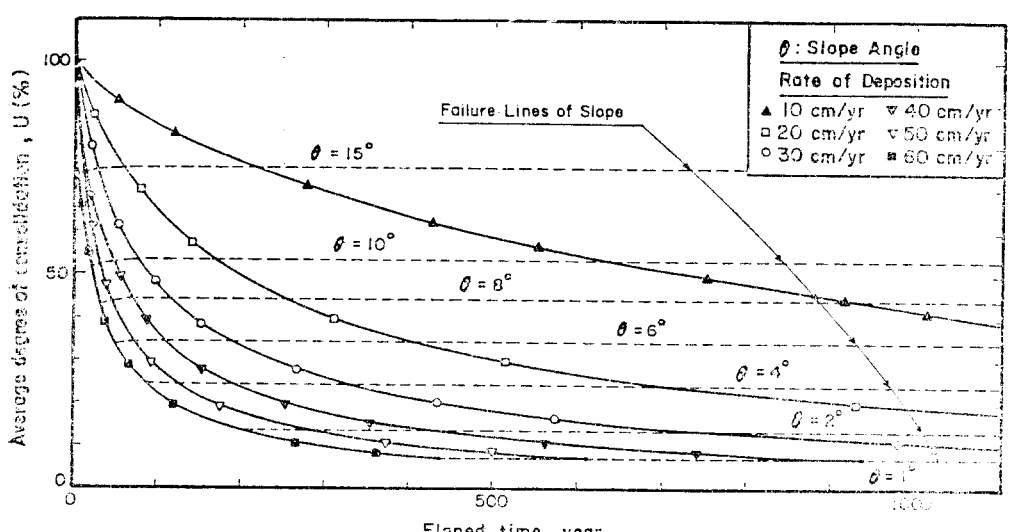

Fig. 16 Degree of consolidation and rate of deposition with time

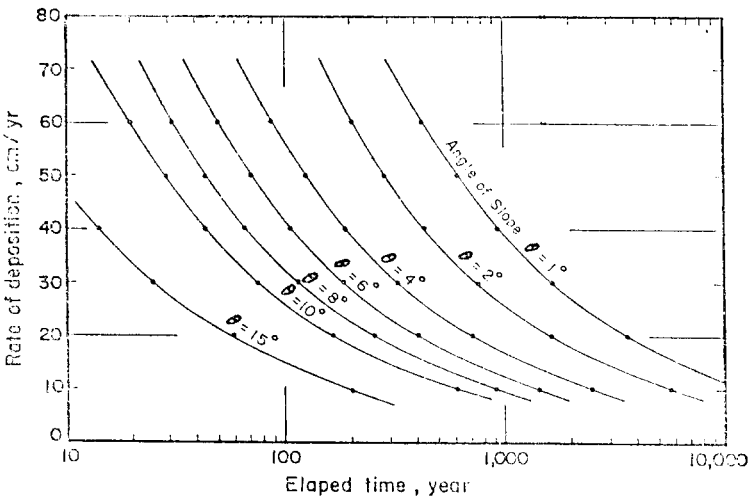

Fig. 17 Expecting time of slope failure and rate of deposition

variation in soil compressibility and permeability during the consolidation process.

5.2 Degree of Consolidation with Time and Rate of Deposition

The relationship between degree of consolidation and time with different rates of deposition was established as shown in Fig. 16. The average pore pressure, u, of deposit gradually decreases with increasing time. It was found through FEM analysis that the pore pressure within submarine deposit is not only a function of time, but also a function of the rate of deposition. Thus, the degree of consolidation decreases as the rate of deposition increases in the same period of time. These results are quite resonable for the soil which has a low permeability. However, this result shows a different trend from the results obtained by OLSSON.[7] This difference is probably caused by the simplifying assumptions which was adopted in the equation.

5.3 Critical State of Slope Stability

The stability of inclined sediment was evaluated using infinite slope analysis. The limit equilibrium concept in which the mass movement occurs on a plane parallel to the seafloor when the shear stress acting downslope exceeds the sediment strength was used. The pore pressures and total stresses were calculated throughout the deposit by solving a series of simultaneous equations. Consequently, the distribution of factor of safety in the vertical direction in deposit was obtained.

Figure 17 illustrates the potential time of failure corresponding to the rate of deposition at any geometry of the infinite slopes.

5.4 Potential Failure Plane

The potential failure plane in time-dependent deposit was located slightly below the middle of the deposit. It was found, however, that the average degree of consolidation at failure for a given angle of slope was identical. The unstable zone at any angle of slope and rate of deposition

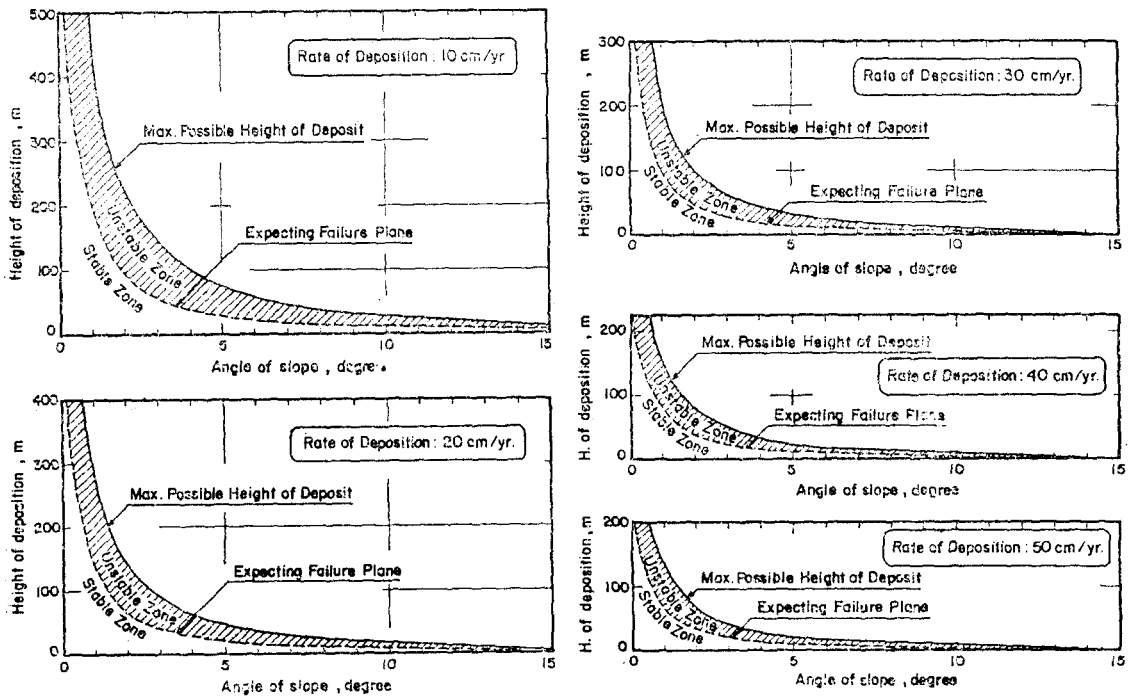

Fig. 18 Rate of deposition and unstable zone

was established as shown in Fig. 18.

If the angle of slope and the rate of deposition are known, the failure time of slope and volume of moving mass of soil can be estimated by Fig. 18. When the angle of the slope and rate of deposit decrease, the volume of moving mass of soil increases.

6. Conclusion

Some behaviours of artificially consolidated clay with a different degree of consolidation and the stability of the submarine seabed undergoinga rapid deposition were studied. The following results were obtained.

(1) The undrained shear strength of clay parabolically increased convexing downward with the degree of consolidation.

(2) The degree of consolidation did not affect the effective strength parameters.

(3) The pore water pressure development during shearing was only a function of effective stress of which the sample had just before shearing.

(4) The degree of consolidation of submarine deposit subjected to constant rate of deposition gradually decreases with increasing time and rate of deposition.

(5) The infinite slope stability analysis showed a straight failure surface which is located slightly below the middle of the deposit.

(6) The volume of moving soil mass increases with decreasing angle of slope and rate of deposition.

7. Acknowledgement

The experimental and numerical work in this paper was carried out at the Asian Institute of Technology. The author wishes to thank his advisor, Dr. I. Towhata for his unstinted help and invaluable guidance.

References

1. BEA, R.G. (1971), "How Seafloor Slides Effect Offshore Structure," *Oil and Gas Journal,* Vol. 69, No. 48, pp. 88~92.
2. BJERRUM, L. (1971), *Subaqueous Slope Failures in Norwegian Fjords,* NGI, Publication No. 88.
3. GIBSON, R.E. (1958), "The Progress of Consolidation in a Clay Layer Increasing in Thickness with Time," *Geotechnique,* Vol. 8, pp. 171~182.
4. KIM, S.R. (1987), *Undrained Shear Strength of Underconsolidated Clay,* M. Eng. Thesis, GT-86-20, AIT, Bangkok.
5. KOLB, C.R. and KAUFMAN, R.I. (1967), "Prodelta Clays of Southeast Louisiana," *Marine Geotechnique,* University of Illinois Press, pp. 3~21.
6. MURTY, T.S. (1979), "Submarine Slide-generated Water Wave in Kitimat Inlet," British Columbia, *Journal of Geophysical Research 84,* pp. 7777~7779.
7. OLSSON, R.G. (1953), "Approximate Solution of the Progress of Consolidation in a Sediment," *3rd ICSMFE Session 1/9,* Switzerland.
8. SANGREY, D.A. (1977), "Marine Geotechnology-State of the Art," *Marine Geotechnology,* Vol. 2, pp. 45~79.
9. SAXOV, S. and NIEUWENHUIS, J.K. Eds. (1982), *Marine Slides and Other Mass Movement,* Plenum Press, N.Y.
10. TERZAGHI, K. (1957), *Varieties of Submarine Slope Failures,* NGI Publication No. 25, pp. 1~16, Oslo.

(접수일자 1988. 7. 29)